PNAS PLUS

Rational design and validation of a vanilloid-sensitive TRPV2 ion channel

Fan Yang (杨帆)[a,1], Simon Vu[a,1], Vladimir Yarov-Yarovoy[a], and Jie Zheng (郑劼)[a,2]

[a]Department of Physiology and Membrane Biology, University of California, Davis, CA 95616

Edited by Richard W. Aldrich, The University of Texas at Austin, Austin, TX, and approved May 12, 2016 (received for review March 14, 2016)

Vanilloids activation of TRPV1 represents an excellent model system of ligand-gated ion channels. Recent studies using cryo-electron microcopy (cryo-EM), computational analysis, and functional quantification revealed the location of capsaicin-binding site and critical residues mediating ligand-binding and channel activation. Based on these new findings, here we have successfully introduced high-affinity binding of capsaicin and resiniferatoxin to the vanilloid-insensitive TRPV2 channel, using a rationally designed minimal set of four point mutations (F467S–S498F–L505T–Q525E, termed TRPV2_Quad). We found that binding of resiniferatoxin activates TRPV2_Quad but the ligand-induced open state is relatively unstable, whereas binding of capsaicin to TRPV2_Quad antagonizes resiniferatoxin-induced activation likely through competition for the same binding sites. Using Rosetta-based molecular docking, we observed a common structural mechanism underlying vanilloids activation of TRPV1 and TRPV2_Quad, where the ligand serves as molecular "glue" that bridges the S4–S5 linker to the S1–S4 domain to open these channels. Our analysis revealed that capsaicin failed to activate TRPV2_Quad likely due to structural constraints preventing such bridge formation. These results not only validate our current working model for capsaicin activation of TRPV1 but also should help guide the design of drug candidate compounds for this important pain sensor.

TRPV1 | TRPV2 | resiniferatoxin | capsaicin | ligand gating

Ion channels constitute the second largest family of drug targets for therapeutics (1–3); therefore, understanding their gating mechanisms by small-molecule ligands is critical for both basic and translational research. Capsaicin activation of the pain-sensing transient receptor potential vanilloid 1 (TRPV1) ion channel represents an outstanding model system for understanding ligand-dependent gating process (4), because capsaicin not only potently activates the channel with a submicromolar EC_{50} (5) but also effectively stabilizes the channel at high open probability (6–8). Moreover, capsaicin activation is highly selective for TRPV1 channel (5). Previous mutagenesis (9, 10) and cryo-EM studies (11, 12) have shown that capsaicin binds near the third (S3) and fourth (S4) transmembrane segments of TRPV1 (Fig. 1*A*). Based on the high-resolution cryo-EM structures, we have used a combination of computational and functional assays to reveal that capsaicin takes a "tail-up, head-down" configuration in the ligand-binding pocket (6) (Fig. 1*B*). The aliphatic tail forms extensive but nonspecific van der Waals (VDW) interactions with residues lining the binding pocket, whereas the vanillyl group (head) and the amide group (neck) of capsaicin form a hydrogen bond with E571 on S4–S5 linker and T551 on S4, respectively. To activate TRPV1, VDW interactions first secure capsaicin in the pocket and the neck of capsaicin forms a hydrogen bond with T551. This is followed by the formation of another hydrogen bond between the head and E571, which stabilizes the outward conformation of S4–S5 linker to open the channel. Although this framework of ligand-gating mechanism is widely supported by the latest computational studies (13–15), further functional tests are needed.

One of the best approaches to validate mechanistic understandings is to experimentally test predictions of the working model. Therefore, we decided to try introducing vanilloid sensitivity to other TRP channels by rationally designed point mutations based on the understanding of how capsaicin activates TRPV1. TRPV2 was chosen as our target because it is the closest homolog to TRPV1 (16), with 43% amino acid sequence identity in the transmembrane domains where the capsaicin-binding pocket is located. Similar to TRPV1, TRPV2 is a polymodal receptor activated by noxious heat, membrane depolarization, and ligands (16). TRPV2 is insensitive to capsaicin. Transplanting the entire S2–S4 domains of TRPV1 into TRPV2 yielded a chimeric channel capable of binding radioactive resiniferatoxin (RTX) (9), another vanilloid molecule produced by the plant euphorbia (Fig. 1*C*) (17). This finding confirmed the overall structural similarity between TRPV1 and TRPV2 (11, 18, 19), which would permit introduction of capsaicin binding to TRPV2. Rather than transferring the entire capsaicin-binding pocket as in the previous study (9), here, we aim to convey vanilloid sensitivity to TRPV2 with minimal structural perturbations by rationally mutating critical residues we identified to be essential for ligand gating of TRPV1 (6).

Results

Rational Design of Point Mutations in TRPV2. Previous studies identified several residues important for capsaicin activation of TRPV1 (6, 9, 10). To first test whether these residues are conserved, we analyzed the amino acid sequence of experimentally confirmed capsaicin-sensitive TRPV1 channels and functional TRPV2 channels from multiple species. We identified four amino acids in TRPV2 that exhibit a dramatic switch in physical properties at critical sites for capsaicin activation (Fig. 1*D* and Figs. S1 and S2). The small polar residue S513 in TRPV1, which is in close proximity to the head of bound capsaicin (6), corresponds to a bulky hydrophobic phenylalanine (F467) in TRPV2 that would most likely impair capsaicin binding due to steric hindrance (6, 9). The

Significance

Understanding how small molecules regulate activities of ion channels, which form the second largest family of drug targets, is important for both basic and translational research. By learning from how capsaicin activates TRPV1, we have introduced high-affinity binding of both capsaicin and resiniferatoxin to TRPV2 with only four point mutations. This successful outcome not only validated the working model for capsaicin–TRPV1 interactions but also suggested that vanilloids such as resiniferatoxin use a similar structural mechanism. Our findings further revealed previously unrecognized structural requirements for capsaicin-induced TRPV1 activation, which will guide future efforts to design drug candidates targeting this important pain sensor. In addition, the modified TRPV2–resiniferatoxin pair has the potential to be further engineered as a tool for chemogenetic studies.

Author contributions: F.Y. and J.Z. designed research; F.Y. and S.V. performed research; F.Y., S.V., V.Y.-Y., and J.Z. analyzed data; and F.Y. and J.Z. wrote the paper.

The authors declare no conflict of interest.

This article is a PNAS Direct Submission.

[1]F.Y. and S.V. contributed equally to this work.

[2]To whom correspondence should be addressed. Email: jzheng@ucdavis.edu.

This article contains supporting information online at www.pnas.org/lookup/suppl/doi:10.1073/pnas.1604180113/-/DCSupplemental.

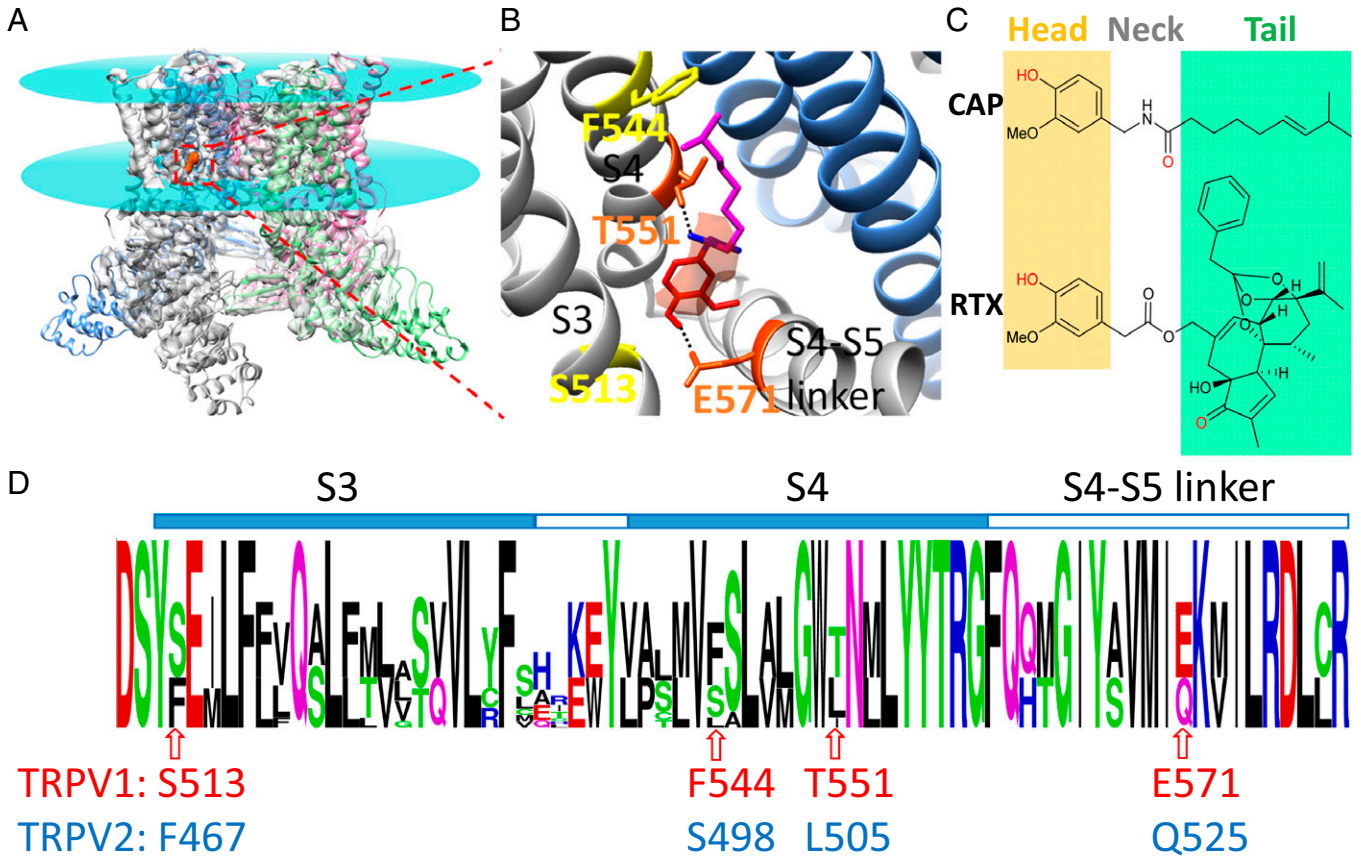

Fig. 1. Rational design of point mutations in TRPV2 to introduce vanilloid sensitivity. (*A*) Cryo-EM structure of TRPV1 (model 3J5R in PDB; electron density map, 5777 in EMD) shows that capsaicin (electron density colored in orange) binds to the transmembrane domains. Lipid membrane boundaries are indicated by cyan disks. (*B*) Binding configuration of capsaicin. Two residues (in orange), T551 on S4 and E571 on the S4–S5 linker, form a hydrogen bond with the neck and head of capsaicin, respectively. Another two key residues, S513 and F544, are shown in yellow. (*C*) Comparison of chemical structures of capsaicin and resiniferatoxin. The vanillyl head and tail groups are shades in yellow and green, respectively. The =O and –OH groups predicted to form a hydrogen bond with TRPV1 are shown in red. (*D*) Sequence logo of the alignment between TRPV1 and TRPV2 channels. The height of a letter is proportional to the relative frequency of that residue at a particular site. Polar residues are colored in green, hydrophobic residues in black, positively charged residues in blue, and negatively charged residues in red. Four key residues designated for mutagenesis are marked by an arrow, with the corresponding residues in TRPV1 and TRPV2 shown in red and blue, respectively.

hydrophobic F544 in TRPV1 participates in VDW interactions with the hydrophobic tail of capsaicin (6), whereas the corresponding residue in TRPV2 is a hydrophilic serine. T551 in TRPV1 forms a hydrogen bond with the neck of capsaicin to stabilize its binding (6), but in TRPV2, the corresponding residue is a hydrophobic leucine incapable of forming a hydrogen bond. The negatively charged E571 in TRPV1 also forms a hydrogen bond with the head of capsaicin to both stabilize the binding and the open state of TRPV1 (6); however, in TRPV2 the corresponding residue is an uncharged glutamine. The remaining residues lining the ligand-binding pocket are either identical or similar. Therefore, differences in the four key residues may explain capsaicin insensitivity in TRPV2.

Not only are the above differences in critical residues drastic in terms of their physical properties, but also such changes occur in a binary manner: residues critical for capsaicin sensitivity in TRPV1 are conserved throughout species, whereas the residues disfavoring capsaicin activation are highly conserved throughout species in TRPV2 (Fig. 1*D* and Fig. S1). Such a binary distribution of the relative frequency of residues allowed substitution of all four sites in TRPV2 with corresponding favoring residues simultaneously. Moreover, during this study, a high-resolution cryo-EM structure model of TRPV2 was reported (18). To further validate our design of point mutations, we compared the structures of TRPV1 and TRPV2. We observed that the four disfavoring residues in TRPV2 identified by multiple sequence alignment (Fig. 1*D*) indeed overlap reasonably well with the critical sites in TRPV1 when these two channel structures are aligned, whereas the overall structure of capsaicin-binding pocket of TRPV1 is similar to the corresponding region of TRPV2 (Fig. 2*A*). Based on our rational design, we generated a TRPV2_Quad mutant containing four point mutations (F467S–S498F–L505T–Q525E), which was then experimentally tested as below.

TRPV2_Quad Is Activated by Resiniferatoxin but Antagonized by Capsaicin. We tested whether TRPV2_Quad could be activated by capsaicin as we designed above. With patch-clamp recording in both whole-cell and inside-out configurations, we first confirmed that TRPV2_Quad channels were activated by a nonselective agonist, 2-aminoethoxydiphenyl borate (2-APB), for TRP channels including the wild-type TRPV2 (20) (Fig. 2 *B* and *C*), indicating that the quadruple mutant channel was functional. However, TRPV2_Quad was not activated by up to 10 μM capsaicin (Fig. 2B). Concentrations higher than 10 μM were not attempted because capsaicin and other lipophilic molecules at higher concentrations will nonspecifically alter the activity of ion channels through perturbation of the membrane (21).

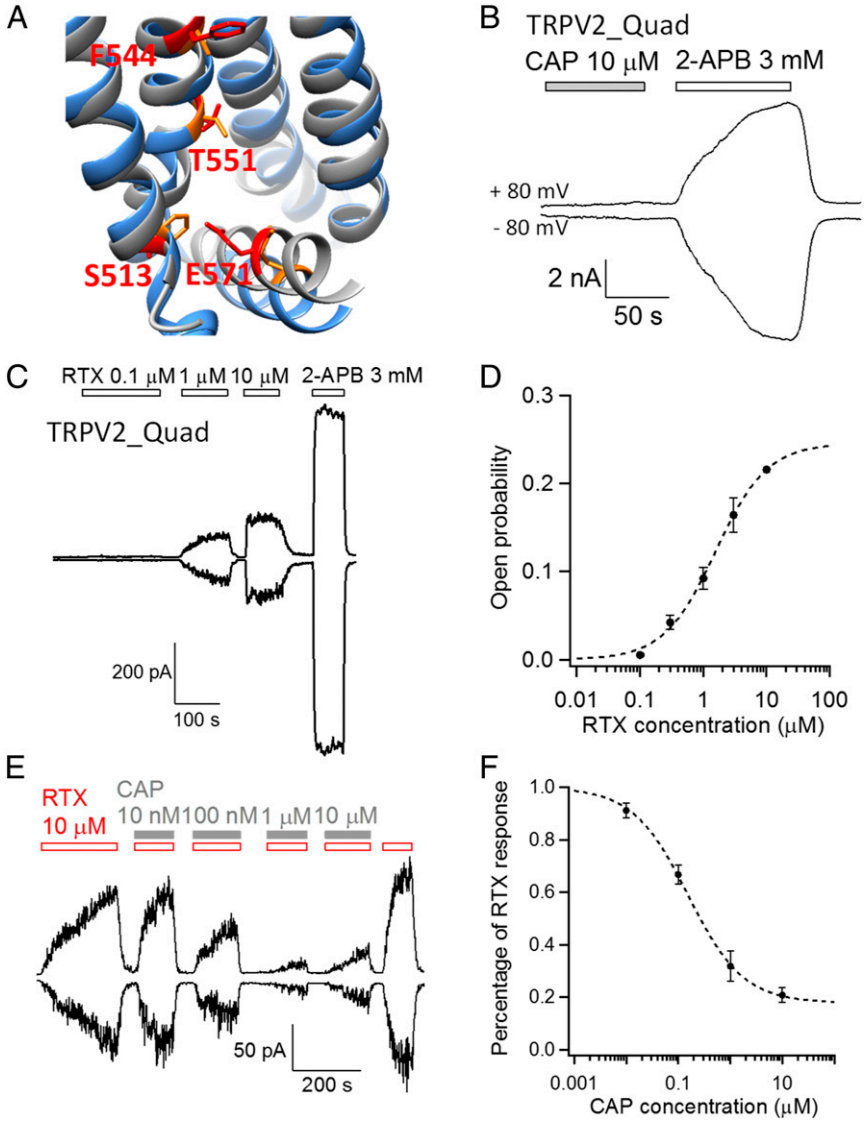

Fig. 2. TRPV2_Quad is sensitive to resiniferatoxin. (*A*) The capsaicin-binding pocket of TRPV1 (gray; PDB ID code 3J5R) is structurally aligned with that of TRPV2 (blue; PDB ID code 5AN8), with the side chain of the four key residues shown in red and orange, respectively. (*B*) An example whole-cell recording demonstrates that TRPV2_Quad was not activated by capsaicin up to 10 μM, whereas 2-APB activated the channels in the same membrane patch. (*C*) Resiniferatoxin activates TRPV2_Quad in a concentration-dependent manner in an inside-out patch. (*D*) Averaged concentration dependence of resiniferatoxin activation ($n = 9$) is fitted to a Hill equation with the following parameters: EC_{50}, 1.4 ± 0.2 μM; Hill coefficient, 1.5 ± 0.1. The resiniferatoxin responses are normalized to the 2-APB response of the same membrane patch. (*E*) Capsaicin antagonizes resiniferatoxin activation of TRPV2_Quad in a concentration-dependent manner in an inside-out patch. (*F*) Averaged concentration dependence of capsaicin inhibition ($n = 5$) is fitted to a Hill equation with the following parameters: IC_{50}, 146.7 ± 15.2 nM; Hill coefficient, 0.7 ± 0.1. Note that, with increasing concentration of capsaicin, resiniferatoxin activation takes a longer time to reach equilibrium, which may lead to underestimation of the value of IC_{50}.

Resiniferatoxin is an extremely potent agonist of TRPV1 (5, 17) and similar to capsaicin in many aspects. Chemically, resiniferatoxin has the same vanillyl "head" group as capsaicin, but with a much larger daphnane tail (Fig. 1*C*). A cryo-EM study revealed that resiniferatoxin binds to the similar pocket in TRPV1 as capsaicin (12). Within this binding pocket, a previous study suggested that resiniferatoxin also takes a tail-up, head-down configuration similar to that of capsaicin (13). Given the ultrahigh potency of resiniferatoxin ($EC_{50} < 1$ nM, about two to three orders of magnitude lower than capsaicin) (22) and its similar binding mode as capsaicin, we decided to test whether TRPV2_Quad, originally designed for capsaicin activation, could be instead activated by resiniferatoxin.

Indeed, we found that resiniferatoxin activates TRPV2_Quad channels. Although wild-type TRPV2 was not activated by resiniferatoxin at up to 10 μM concentration (Fig. S3), 1 μM resiniferatoxin could clearly activate TRPV2_Quad (Fig. 2*C*). Although TRPV1 is activated by resiniferatoxin at much lower concentrations, resiniferatoxin irreversibly binds to TRPV1 and could not be washed off (Fig. S3), which largely limits its utility as a tool to investigate the biophysical properties of the channel. In contrast, resiniferatoxin activation of TRPV2_Quad could be rapidly and completely reversed by wash-off (Fig. 2*C*), allowing channel activation to be examined under equilibrium conditions. TRPV2_Quad activation by resiniferatoxin occurred in a concentration-dependent manner (Fig. 2 *C* and *D*). By fitting the data to a Hill equation, the EC_{50} was determined to be 1.4 ± 0.2 μM ($n = 9$). The Hill coefficient for channel activation was 1.5 ± 0.1 ($n = 9$), suggesting that likely more than one resiniferatoxin molecule binds to activate the channel. At near-saturating

concentrations, current amplitude attained by resiniferatoxin was about one-fourth of that by 2-APB (Fig. 2*D*), indicating that resiniferatoxin is a partial agonist of TRPV2_Quad. Therefore, we successfully introduced resiniferatoxin sensitivity to TRPV2 channel by only four point mutations.

As capsaicin and resiniferatoxin share similar chemical structure in the head and neck region, we wondered whether capsaicin could bind to TRPV2_Quad like resiniferatoxin but failed to activate the channel. To test this possibility, we coapplied resiniferatoxin and capsaicin on TRPV2_Quad (Fig. 2*E*). Indeed, we observed that current induced by 10 μM resiniferatoxin was antagonized by capsaicin in a concentration-dependent manner, with an IC_{50} value of 146.7 ± 15.2 nM (n = 5). At saturating concentration (10 μM), capsaicin was able to inhibit 83.4 ± 3.9% of resiniferatoxin-induced current from TRPV2_Quad (n = 4) (Fig. 2 *E* and *F*), while having no significant effect on 2-APB–induced current from wild-type TRPV2 or TRPV3 channels (Fig. S4). These observations revealed that capsaicin serves as an antagonist of TRPV2_Quad by competing with resiniferatoxin for the same introduced vanilloid-binding sites.

TRPV2_Quad Behaves as an OFF Switch. Not only was TRPV2_Quad directly activated by resiniferatoxin, but also we observed a peculiar current response from the channel: when the ligand was rapidly washed off after reaching steady state, the current exhibited a rapid surge before declining back to the background level (Fig. 3*A*). We called such current response an OFF response. This OFF response in TRPV2_Quad was observed when 2-APB was first applied to activate the channel (n = 6). Although the 2-APB–induced current completely reversed upon wash-off before resiniferatoxin was applied to the same channels, apparently 2-APB may have tuned the channels into a different state to allow an OFF response. Unlike the steady-state current induced by resiniferatoxin, which was much smaller than the 2-APB–induced response (Fig. 2 *C* and *D*, and Fig. 3*A*), the OFF response from 1 μM resiniferatoxin had a peak amplitude similar to that of 2-APB. Applying resiniferatoxin to mutant TRPV2 channels containing only two (F467S_L505T) or three (F467S_S498F_L505T) of the quadruple mutants yielded very weak current responses in steady state, but detectable OFF response similar to TRPV2_Quad (Fig. S5). These observations suggest that resiniferatoxin can indeed effectively open TRPV2_Quad, although such an open state is unstable.

We investigated the mechanism underlying the OFF response of TRPV2_Quad. Previously, we observed that when proton was used to activate TRPV1 and then was quickly washed off, a similar OFF response occurred (23). We found that this TRPV1 OFF response was caused by rapid removal of proton block of the channel pore during wash-off when proton-induced channel activation had not deactivated (23). Therefore, we first tested whether a pore blockade mechanism is also applicable to resiniferatoxin-induced OFF response in TRPV2_Quad. We found that the single-channel conductance values of TRPV2_Quad activated by either resiniferatoxin (120.9 ± 1.4 pS; n = 4) or 2-APB (119.9 ± 3.7 pS; n = 4) were similar (P = 0.82) (Fig. S6). Therefore, the OFF response of TRPV2_Quad is unlikely due to removal of pore blockage by resiniferatoxin.

Noticeably, the OFF response behavior of TRPV2_Quad closely resembles the repolarizing I_{kr} current through human ether-à-go-go–related gene (hERG) channels in heart (24, 25). The I_{kr} current of

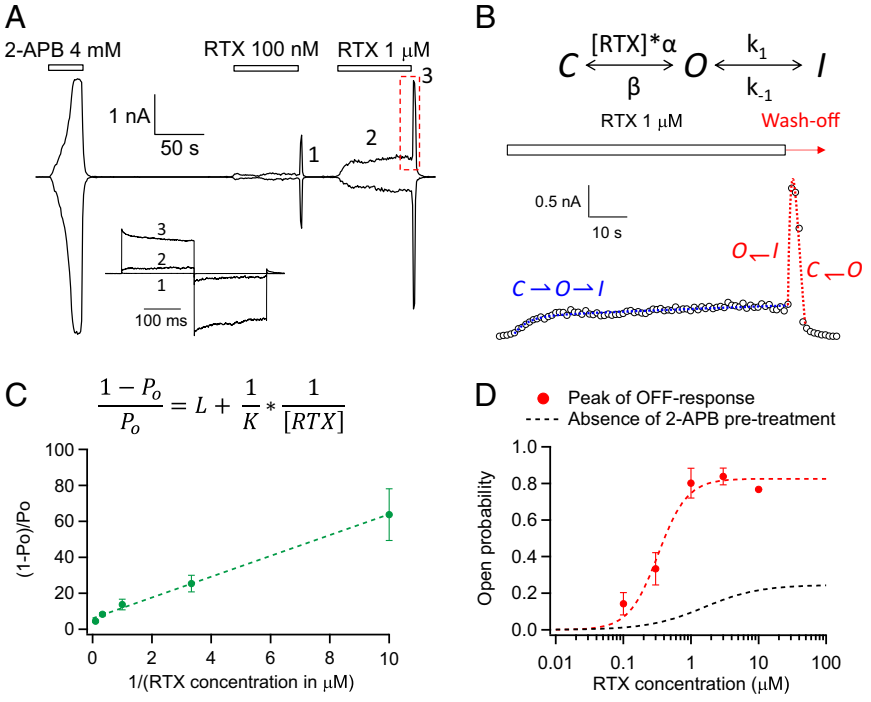

Fig. 3. Resiniferatoxin-induced TRPV2_Quad activation exhibits a large OFF response. (*A*) TRPV2_Quad pretreated with 2-APB yielded a large transient current surge (marked with a red dashed box) upon removal of resiniferatoxin. Representative current traces at labeled time points are shown in *Inset*. (*B*) A three-state gating model is sufficient to recapitulate the time course of the resiniferatoxin-induced TRPV2_Quad response. A double-exponential function dictated by such a gating model with two similar time constants such as 1.1 and 0.9 s was able to recapitulate the OFF response (dashed red trace). (*C*) Based on the three-state gating model shown in *B*, the concentration dependence of steady-state open probability (Po) before wash-off is fitted to determine K and L, the resiniferatoxin binding affinity, and the equilibrium constant for the $O \leftrightarrow I$ transition, respectively (see *Materials and Methods* for details). K = 203.7 ± 36.1 nM^{-1}; L = 4.9 ± 1.3. (*D*) Averaged concentration dependence of the peak OFF response (red symbols; n = 6) is fitted to a Hill equation with an EC_{50} value of 222.9 ± 44.3 nM (n = 6). The concentration–response curve without pretreatment of 2-APB (Fig. 2*D*) is reproduced here as the black dashed curve. Open probability is calculated by normalizing resiniferatoxin responses to the 2-APB response of the same membrane patch as the open probability achieved by 2-APB was determined by noise analysis (Fig. S7).

hERG channels is critical for controlling heart rate and rhythm; disrupting I_{kr} by either hERG mutations or drugs leads to severe diseases such as long QT syndromes (26). Upon activation by depolarization (equivalent to agonist activation of TRPV2_Quad), hERG channels quickly inactivate, yielding a low steady-state open probability. However, when the membrane potential is repolarized (equivalent to resiniferatoxin wash-off for TRPV2_Quad), hERG channels transit from the inactivated state back to the open state to give rise to a large current spike similar to the OFF response from TRPV2_Quad. Indeed, a three-state gating model (see *Materials and Methods* for details) nicely recapitulated both the kinetic properties (Fig. 3*B*) and the equilibrium properties (Fig. 3*C*) of TRPV2_Quad. The analysis further suggested that the highest open probability TRPV2_Quad can attain at saturating ligand concentrations is limited because the I state is more stable than the O state (L being about 5). To measure such an open probability, the maximum open probability of TRPV2_Quad activated by 2-APB was determined by noise analysis (83.7 ± 2.7%; n = 6) (Fig. S7). To calculate resiniferatoxin-induced open probability, its current amplitude in the steady state was then normalized to the 2-APB response. In addition, the ligand-binding affinity (K) estimated using the three-state model is 203.7 ± 36.1 nM^{-1} (n = 8) (Fig. 3*C*, inverse of the slope of fitted linear function), whereas the EC_{50} value measured from the concentration dependence of peak OFF response is 222.9 ± 44.3 nM (n = 6) (Fig. 3*D*). Our data thus revealed that TRPV2_Quad could bind resiniferatoxin with at least a low micromolar affinity but failed to yield a stable open state due to the existence of a more stable nonconducting state. Therefore, the quadruple mutation successfully introduced high-affinity vanilloid binding into TRPV2.

Resiniferatoxin Serves as Molecular "Glue" Between the S4–S5 Linker and S1–S4 Domain to Activate TRPV2_Quad and TRPV1 Channels. As TRPV2_Quad, which was originally designed to be capsaicin sensitive, is activated only by resiniferatoxin but antagonized by capsaicin, we investigated the underlying structural mechanism. We first analyzed the physical properties of the capsaicin-binding pocket in TRPV1, as well as the corresponding regions in TRPV2 and TRPV2_Quad. In all three channels, we observed that this pocket exhibited generally similar electrostatics and hydrophobicity distributions, with uncharged and hydrophobic residues located within the membrane region while charged and hydrophilic residues concentrated at the interface with aqueous environment (Fig. 4). Particularly, Q525E and S498F in TRPV2_Quad tune the pocket to more closely resemble TRPV1. Apparently, minor differences in electrostatics and hydrophobicity are insufficient to explain the distinct responses of TRPV2_Quad to resiniferatoxin and capsaicin.

With the newly available TRPV2 cryo-EM structure, we did find one noticeable difference: TRPV2's ligand-binding pocket is substantially larger in volume (1,242.2 $Å^3$) than that of TRPV1 (910.6 $Å^3$). As the tail of resiniferatoxin is much larger than that of capsaicin (Fig. 1*C*), resiniferatoxin may be better accommodated in the pocket of TRPV2_Quad with this increased volume. More importantly, when the ligand-binding pocket structures of these two channels were aligned, the S4–S5 linker lining the bottom of the pocket was found to be lower by about 3 Å in TRPV2 relative to TRPV1 (Fig. 5*A*). This shift in the S4–S5 linker position is likely the consequence of one extra helical turn at the end of S4 in TRPV2 (Fig. 5*B*). Downshift of the S4–S5 linker increases the distance between the two residues involved in hydrogen bond formations by 2.4 Å (measured from Cα atoms). It is therefore possible that this unanticipated increase in distance prevented capsaicin from activating TRPV2_Quad.

To test the above hypotheses, we first computationally docked resiniferatoxin into the pocket of TRPV1 using the Rosetta suite with membrane energy functions (6, 27–29). Docking models with the highest binding energies showed structural convergence (Fig. S8), with the resiniferatoxin molecule adopting a tail-up, head-down configuration inside the pocket (Fig. 6*A*). This is a similar pose to the bound capsaicin as we observed previously

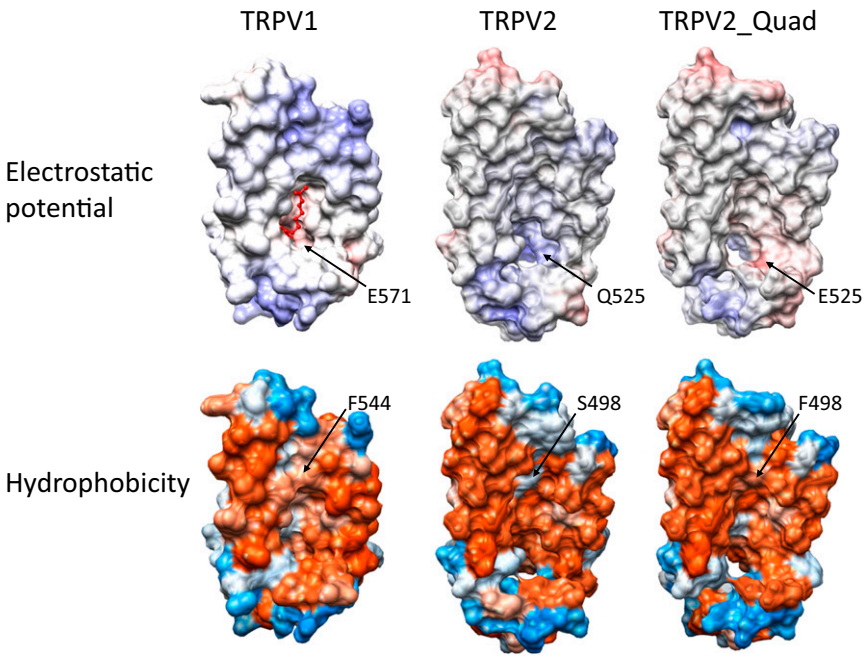

Fig. 4. Similar physical properties observed in the ligand-binding pocket of TRPV1, TRPV2, and TRPV2_Quad. All structures are aligned to the conformation of the capsaicin-binding pocket in TRPV1 (*Top Left*), in which a capsaicin molecule (in red) is shown. Electrostatic potential is calculated by Adaptive Poisson–Boltzmann Solver (APBS) in UCSF Chimera. Positive and negative charged residues are colored in blue and red, respectively. Hydrophobicity is calculated based on the Kyte and Doolittle scale in UCSF Chimera. Hydrophobic and hydrophilic residues are colored in orange and blue, respectively. Two (S498F and Q525E) of the four mutations in TRPV2_Quad, as well as their corresponding wild-type residues, are marked by an arrow.

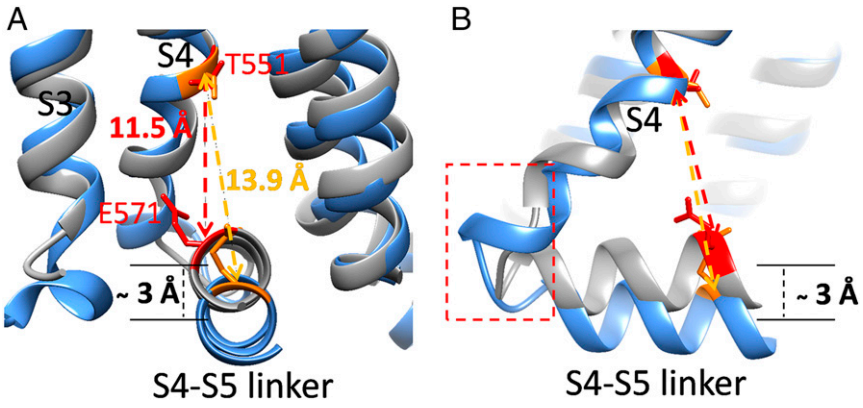

Fig. 5. Structural difference in the binding pockets of TRPV1 and TRPV2. (*A*) Front view of the ligand-binding pocket, with TRPV1 and TRPV2 shown in gray and blue, respectively. With their structures aligned by the S1–S4 domains, the S4–S5 linker of TRPV2 is about 3 Å lower than that of TRPV1. This leads to a 2.4-Å difference in distance between T551 and E571 in TRPV1 (colored in red; 11.5 Å) compared with that of the corresponding residues in TRPV2 (colored in orange; 13.9 Å). (*B*) Side view of the pocket. The lowering of S4–S5 linker in TRPV2 is accompanied with an extra helical turn at the end of S4 (indicated by a red dashed box).

(Fig. 6*B*) (6). Moreover, the docked resiniferatoxin in a recent study adopted a similar configuration as we observed here (13). In our docking models, the tail of resiniferatoxin agreeably overlapped with the experimentally observed electron density in the cryo-EM structure (Fig. 6*A*, yellow surface) (12). The fact that no electron density represents the resiniferatoxin head may suggest that this part of the molecule takes more than one position—a situation reminiscent of the capsaicin tail in the TRPV1 ligand-binding pocket (6, 13).

Upon closer inspection, we found that T551 in S4 forms a hydrogen bond with an oxygen atom (Fig. 1*C*, colored in red) on the tail of resiniferatoxin (Fig. 6*A*, dashed line), which would contribute to the stabilization of resiniferatoxin inside the pocket. We previously observed that T551 also makes a hydrogen bond with capsaicin to stabilize its binding. However, the hydrogen bond is formed with the oxygen atom on the capsaicin neck (6). The resiniferatoxin neck is made of an ester instead of an amide found in capsaicin. This change in chemical structure may affect the stability of a potential hydrogen bond formed with the S4 threonine. Furthermore, in resiniferatoxin, the associated shortening in distance between the =O group in the neck and the –OH group in the head may also prevent simultaneous formation of hydrogen bonds with S4 and the S4–S5 linker. The oxygen in resiniferatoxin tail is further away from the head, thus alleviating the distance constrain. We further observed that the head of resiniferatoxin forms hydrogen bonds with E571 on S4–S5 linker and S513 on S3 (Fig. 6*A*, dashed lines), which glues the S4–S5 linker to the anticipated stationary S1–S4 domain (30). Hence, although different parts of vanilloids are involved in interactions with TRPV1, the underlying activation mechanism appears to be analogous for capsaicin and resiniferatoxin (Fig. 6*B*) (6).

We next examined how resiniferatoxin interacts with TRPV2_Quad. We observed that resiniferatoxin was able to enter the binding pocket in TRPV2_Quad as it stayed stably behind Y466, which marks the entrance of the binding pocket (Fig. 6*C*, gray). The corresponding residue (Y512) in TRPV1 is also positioned at the entrance of the ligand-binding pocket (Fig. 6*A*, gray) (11). Inside the pocket, the tail of resiniferatoxin forms a hydrogen bond with T551 as it does in TRPV1 (Fig. 6*C*). The head of resiniferatoxin also forms hydrogen bonds with residues in the S4–S5 linker (S521) and the end of S4 (T511 and R512) (Fig. 6*C*), gluing these helices together. In contrast, we observed that resiniferatoxin was unable to stay inside the corresponding pocket of the wild-type TRPV2, with its tail remaining mostly outside the pocket entrance marked by Y466 (Fig. 6*D*). Therefore, resiniferatoxin was able to recapitulate its binding mode in TRPV1 only in TRPV2_Quad owing to the quadruple mutation, with the tail stably binding inside the pocket via the hydrogen bond and VDW interactions and the head bridging between the S4–S5 linker and the S1–S4 domain. The gluing of the S4–S5 linker to the S1–S4 domain by resiniferatoxin appears to enable its activation of TRPV2_Quad channel.

Based on the proposed binding mode of vanilloids in TRPV1 and TRPV2_Quad, we tested whether capsaicin can bind to TRPV2_Quad in a similar manner. Top models of the capsaicin–TRPV2_Quad complex with largest binding energy showed that the neck of capsaicin was able to form a hydrogen bond with T505 (equivalent to T551 on TRPV1) on TRPV2_Quad, with the tail pointing upward (Fig. 6*E* and Fig. S8) (6). However, the head of capsaicin cannot form a hydrogen bond with E525 (equivalent to E571 on TRPV1), preventing the gluing of S4–S5 linker to the S1–S4 domain as capsaicin does in TRPV1 and resiniferatoxin does in TRPV2_Quad. This is likely caused by the lowering of S4–S5 linker in TRPV2 (Fig. 5), which leaves capsaicin unable to reach T505 and E525 simultaneously. Instead, the head is observed to form a network of hydrogen bonds with Y466, S467, and R512 (equivalent to Y512, S513, and R558 on TRPV1, respectively) (Fig. 6*E*), leaving the S4–S5 linker uncontrolled. Therefore, although capsaicin can bind stably to the same pocket in TRPV2_Quad to antagonize resiniferatoxin activation (Fig. 2 *E* and *F*), its altered binding mode fails to stabilize the open state of this channel.

Discussion

We have successfully introduced high-affinity binding of capsaicin and resiniferatoxin to TRPV2 channel by four point mutations, which were rationally designed based on the current understanding of how capsaicin activates TRPV1 (6, 13–15). Although resiniferatoxin activates the designed TRPV2_Quad, capsaicin antagonizes this channel. These results have not only validated the current working model for capsaicin activation (6) but also demonstrated that vanilloid compounds such as capsaicin and resiniferatoxin may use similar structural mechanisms to activate the channel.

In such a common gating mechanism, the vanillyl head points downward toward the interface between lipid membrane and intracellular aqueous environment, where it mediates the interactions between the S1–S4 domain and S4–S5 linker. Here, the bulky sidechain of F467 on S3 of the wild-type TRPV2 would sterically prevent the vanilloid head group from taking such a

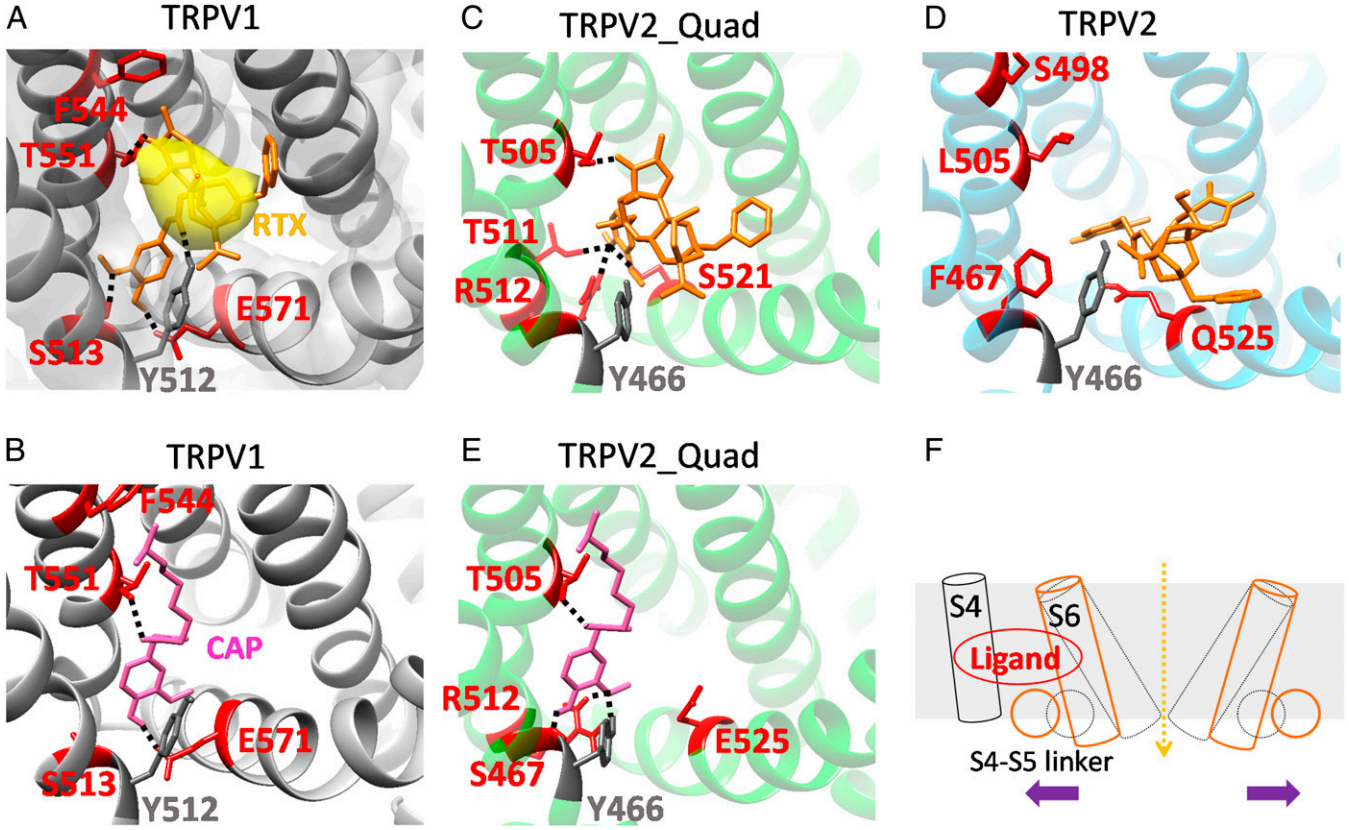

Fig. 6. Docking of vanilloid molecules reveals a common mechanism for ligand activation. For each docking experiment, the model with the lowest binding energy among the converged cluster of top 10 models is shown. (*A*) Docking of resiniferatoxin to TRPV1. The cryo-EM structure of TRPV1 with RTX bound (PDB ID code 3J5Q) was used. The tail of docked resiniferatoxin agreeably overlaps with the experimentally observed electron density (surface colored in yellow; EMD ID 5776). Y512 marks the entrance of the binding pocket. Four critical residues for capsaicin activation are in red. Potential hydrogen bonds between resiniferatoxin and TRPV1 are represented by black dashed lines. (*B*) Docking of capsaicin to TRPV1. (*C*) Docking of resiniferatoxin to TRPV2_Quad. Residues potentially forming hydrogen bonds with resiniferatoxin are in red. Note that resiniferatoxin is able to preserve a similar binding configuration as in TRPV1, with the tail residing inside the binding pocket and the head forming a network of hydrogen bonds. (*D*) Docking of resiniferatoxin to wild-type TRPV2. Unlike in TRPV2_Quad (*C*), resiniferatoxin cannot stay inside the binding pocket, as its tail is outside of Y466, which corresponds to Y512 in TRPV1 that marks the entrance of binding pocket. (*E*) Docking of capsaicin to TRPV2_Quad. Compared with docking in TRPV1 (*B*), the neck of capsaicin still forms a hydrogen bond with T505 (equivalent to T551 on TRPV1). Instead of E525 in the S4–S5 linker, multiple potential hydrogen bonds are observed between the head and Y466, S467, and R512. (*F*) A cartoon illustrating that a vanilloid ligand, when bound favorably inside the binding pocket, stabilizes the S4–S5 linker toward S4, leading to the repositioning of S6 to open the TRP channel.

favorable position. When F467 was mutated to a less bulky residue such as serine in TRPV1, the head can enter and form multiple hydrogen bonds to the S1–S4 domain and S4–S5 linker (Fig. 6*C*). In agreement with this view, when the TRPV1 S513 was mutated to a tyrosine with a similarly bulky side chain as phenylalanine, capsaicin activation was largely disrupted (6, 9). To stabilize ligand binding, the tail of vanilloid compound forms VDW interactions with the channel inside the ligand-binding pocket (6). In TRPV2_Quad, the tail of resiniferatoxin resides favorably inside the pocket, partially because the introduced T505 can form a hydrogen bond with the tail (Fig. 6*C*). In TRPV1, the corresponding residue T551 also makes a hydrogen bond with capsaicin to stabilize its binding (6). However, in wild-type TRPV2, a leucine presents at the corresponding position, whose side chain is unable to form a hydrogen bond. Indeed, our docking experiments suggested that resiniferatoxin stays outside of the bind pocket and cannot activate wild-type TRPV2 (Fig. 6*D*). Therefore, for vanilloid binding, both spatial accommodation and energy stabilization through the formation of VDW interactions and hydrogen bonds are required.

Upon binding of a vanilloid compound, the ligand works as glue to bridge the S1–S4 domain and the S4–S5 linker and activate the channel (Fig. 6*F*). Indeed, our docking of resiniferatoxin suggested that it forms a network of hydrogen bonds between the S1–S4 domain and S4–S5 linker, which is likely to stabilize permissive conformation of the linker to activate TRPV1 as well as TRPV2_Quad. In contrast, although docking shows the neck of capsaicin forms a hydrogen bond with TRPV2_Quad, its head cannot reach and stabilize the S4–S5 linker toward the S1–S4 domain. The formation of a single hydrogen bond without bridging supports capsaicin binding but not capsaicin-induced activation conformational changes, rendering capsaicin an antagonist but not an agonist of TRPV2_Quad. In support of this view, existing studies have shown that, when the head of vanilloid compounds was chemically modified by adding Cl, Br, or I atoms that would disrupt its interaction with the S4–S5 linker, these halogenated resiniferatoxin or capsaicin analogs could still bind to TRPV1 but functioned as an antagonist of the channel instead of an agonist (31, 32).

The S4–S5 linker mediates gating motions in many ion channels with six transmembrane domains (33). For voltage-gated potassium (Kv) and sodium (Nav) channels, membrane depolarization causes movements of the voltage sensor S4 (34). Conformational change in S4 is coupled to the movement of the S4–S5 linker to induce a conformational change in S6 interacting with the linker, leading to the opening of the activation gate (35–37). Although the S1–S4 domains of TRP channels are structurally similar to that of Kv

channels (11, 18, 19, 38, 39), no positively charged residue exists in the S4 of TRPV channels so this domain is expected to remain stationary upon membrane depolarization or the presence of other activators (30). This allows capsaicin or resiniferatoxin to first secure itself to the stationary S1–S4 domain, and then stabilize the outward conformation of the S4–S5 linker to mediate S6 movements leading to channel activation (6, 40). In this way, vanilloid-mediated ligand activation of TRPV1 closely mimics voltage activation of Kv and Nav channels. Conformational change in the S4–S5 linker relative to the S1–S4 domain may serve as a general mechanism to open the activation gate, which is driven by either depolarization-induced S4 movements in voltage-gated channels or vanilloid-mediated bridging in TRP channels.

The capability of resiniferatoxin to bind and gate TRPV1 has profound implications in both clinical and basic research. In particular, due to its high potency and specificity for TRPV1, resiniferatoxin has been used as a "molecular scalpel" (41) to permanently ablate pain-sensing neurons highly expressing TRPV1 in both animal models (42–44) and patients with intractable cancer pain (45). Understanding how resiniferatoxin and capsaicin bind and activate TRPV1 would further facilitate development of more effective and selective treatments. Furthermore, with our engineered TRPV2_Quad, its resiniferatoxin sensitivity could be used to manipulate neuronal activities by selectively expressing this channel in TRPV1 knockout animals, which are insensitive to resiniferatoxin (46). Indeed, a previous study has demonstrated that, in TRPV1 knockout mice, by introducing TRPV1 into dopaminergic neurons, capsaicin could be used to modulate neuronal excitability to further control behaviors of the mice (47). Therefore, the resiniferatoxin-TRPV2_Quad system not only has validated our understanding of vanilloid-mediated ligand gating of TRPV1 channels but also has the potential to be further developed as a tool for chemogenetic studies due to the high specificity of resiniferatoxin (48). We suggest that, if coupled with other ion channels, the ligand-driven OFF response from TRPV2_Quad channels may have the potential to set up and tune rhythmic behaviors in excitable cells.

Materials and Methods

Molecular Biology and Cell Transfection. Murine TRPV1 and TRPV2 were used in this study, and all of the numbering of residues is based on these channels. Enhanced yellow fluorescence protein (eYFP) was genetically linked to the C terminus of these channels to facilitate identification of positively transfected cells. Fusion of eYFP does not alter the function of these channels (49). Point mutations were made by QuikChange II mutagenesis kit (Agilent Technologies). All mutations were confirmed by sequencing.

HEK293T cells were purchased from and authenticated by American Type Culture Collection. They were cultured in DMEM supplemented with 20 mM L-glutamine and 10% (vol/vol) FBS. These cells were transiently transfected with cDNA constructs by Lipofectamine 2000 (Life Technologies) following the manufacturer's protocol. Patch-clamp recordings were performed 1–2 d after transfection.

Chemicals. All chemicals, including resiniferatoxin and capsaicin, were purchased from Sigma-Aldrich.

Electrophysiology. Patch-clamp recordings were performed with a HEKA EPC10 amplifier with PatchMaster software (HEKA) in inside-out or whole-cell configuration. Patch pipettes were prepared from borosilicate glass and fire-polished to resistance of ~4 MΩ for recording. For whole-cell recording, serial resistance was compensated by 60%. Solution containing 130 mM NaCl, 10 mM glucose, 0.2 mM EDTA, and 3 mM Hepes (pH 7.2) was used in both bath and pipette. All recordings were performed at room temperature (~24 °C). Temperature variation was less than 1 °C as monitored by a thermometer. Current signal was sampled at 10 kHz and filtered at 2.9 kHz.

To apply resiniferatoxin or other drugs during patch-clamp recording, a rapid solution changer with a gravity-driven perfusion system was used (RSC-200; Bio-Logic). Each solution was delivered through a separate tube so there was no mixing of solutions. Pipette tip with a membrane patch was placed directly in front of the perfusion outlet during recording to ensure solution exchange was complete.

Protein Sequence Analysis. TRPV1 and TRPV2 protein sequences from six and four different species, respectively, were extracted from UniProtKB database (50). All TRPV1 channels included here for sequence analysis are activated by capsaicin as reported in literature (5, 10, 22, 51–53). All TRPV2 channels used have been shown to be functional (16, 18, 54). Multiple sequence alignment of all 10 channels was performed by Clustal Omega (55). The alignment was visualized in Jalview with Zappo color scheme (56). Based on the alignment, the relative frequency of individual amino acid at each position in the transmembrane domains was further analyzed and visualized by WebLogo (57).

Molecular Modeling and Docking. Transmembrane domains of murine TRPV2 and its mutants were modeled by the comparative modeling application in Rosetta program suite (RosettaCM) (58) using the cryo-EM structure of rabbit TRPV2 [Protein Data Bank (PDB) ID code 5AN8] (18) as template. The sequence identity between rabbit and mouse TRPV2 in the transmembrane region is 94%, sufficiently high to ensure accurate homology modeling. A total of 10,000 models were generated by RosettaCM and subsequently relaxed in Rosetta. The model with lowest energy was used for molecular docking. The same procedure was applied to model the transmembrane domains of TRPV2_Quad channel based on rabbit TRPV2 structure (18).

Docking experiments of resiniferatoxin and capsaicin were performed as previously described (6). Briefly, RosettaLigand application (59–61) from Rosetta program suite, version 3.5, was used (27) to dock the molecules. Models of the transmembrane domains of mouse TRPV2, TRPV2_Quad (built as described above), and rat TRPV1 in the capsaicin-bound state (PDB ID code 3J5R) were first relaxed in membrane environment using the RosettaMembrane application (29, 37, 62). Resiniferatoxin or capsaicin molecule was initially placed roughly in the center of the binding pocket defined by S3, S4, S4–S5 linker, and S6 segments. The electron density of resiniferatoxin or capsaicin observed by cryo-EM imaging (12) was not used as constraints for docking. After docking, the top 1,000 models with lowest total energy score were first selected. They were further scored with the binding energy between ligand and the channel. The top 10 models with lowest binding energy were identified as the candidates. The model with lowest binding energy among the largest cluster of the top 10 models was used as the representative model.

The volume of the binding pockets on TRPV1 and TRPV2 was measured by CAVER Analyst, version 1.0 (63). University of California, San Francisco (UCSF) Chimera (64) software, version 1.9, was used to render all graphs of docking models.

Data Analysis. Current recordings were analyzed in Igor Pro, version 5 (WaveMatrix). By fitting experimentally derived concentration–response relationship to a Hill equation, the EC_{50} and Hill coefficient were determined. To describe the transient OFF response seen in 2-APB–pretreated TRPV2_Quad channels when resiniferatoxin was washed off, the following simplified gating scheme was used:

$$C \underset{\beta}{\overset{[RTX]*\alpha}{\rightleftarrows}} O \underset{K_{-1}}{\overset{K_1}{\rightleftarrows}} I.$$

In this model, the affinity of resiniferatoxin for TRPV2_Quad is determined by the ratio between the forward and backward transition rates, α/β, which is further defined as K. The equilibrium constant between the open state (O) and the inactivated state (I) is determined by k_1/k_{-1}, which is denoted as L.

For the channel open probability at the equilibrium state, this model predicts that

$$\frac{1-P_o}{P_o} = L + \frac{1}{K} * \frac{1}{[RTX]}.$$

Therefore, to determine K and L, the steady-state open probability of TRPV2_Quad measured right before resiniferatoxin wash-off was determined at various resiniferatoxin concentrations. The ratio between the closed and open probabilities, $(1-Po)/Po$, was plotted against the inverse of resiniferatoxin concentration. A linear function was used to fit the data, with the K and L values determined as the inverse of the slope and the intercept at the y axis, respectively.

Given that the gating model shown above contains three states, for the time-dependent change in the probability of residing in any state, the model dictates that it follows a double-exponential function (65). Particularly for the time course of the OFF response upon washing off resiniferatoxin, as the concentration of resiniferatoxin becomes negligible, the first forward

transition can be omitted. The time-dependent change in the open probability takes the following general form:

$$P_o(t) = c_1 * e^{-\frac{1}{2}*t*\left(\sqrt{(\beta+k_1+k_{-1})^2-4*k_1*k_{-1}}+\beta+k_1+k_{-1}\right)} + c_2 * e^{\frac{1}{2}*t*\left(\sqrt{(\beta+k_1+k_{-1})^2-4*k_1*k_{-1}}-\beta-k_1-k_{-1}\right)}.$$

Therefore, a double-exponential function was used in Igor Pro to fit the time course of the OFF response.

To estimate the open probability of 2-APB–induced TRPV2_Quad activation, noise analysis (66) was performed as described previously (67). The open probability of TRPV2_Quad activated by resiniferatoxin was estimated from the relative current amplitude in comparison with that of 2-APB–induced current from the same patch. To estimate channel conductance from single-channel recordings, current amplitude measured at –80 mV was estimated from as all-point histogram of single-channel recordings. A dead time of 0.32 ms was imposed.

Statistics. All statistical data are given as mean ± SEM. Student's *t* test was applied to examine the statistical significance. N.S. indicates no significance. $***P < 0.001$.

ACKNOWLEDGMENTS. We are grateful to our laboratory members for assistance and insightful discussions, and Jon Sack for constructive critiques of the manuscript. This work was supported by funding from NIH Grant R01NS072377 (to J.Z.), AHA Grant 14POST19820027 (to F.Y.), and the University of California, Davis, startup fund (to V.Y.-Y.) toward the purchase of a shared computer cluster at the Genome and Biomedical Sciences Facility.

1. Hille B (2001) *Ion Channels of Excitable Membranes* (Sinauer, Sunderland, MA), 3rd Ed.
2. Zheng J, Trudeau MC (2015) *Handbook of Ion Channels* (CRC, Boca Raton, FL).
3. Overington JP, Al-Lazikani B, Hopkins AL (2006) How many drug targets are there? *Nat Rev Drug Discov* 5(12):993–996.
4. Zheng J (2013) Molecular mechanism of TRP channels. *Compr Physiol* 3(1):221–242.
5. Caterina MJ, et al. (1997) The capsaicin receptor: A heat-activated ion channel in the pain pathway. *Nature* 389(6653):816–824.
6. Yang F, et al. (2015) Structural mechanism underlying capsaicin binding and activation of the TRPV1 ion channel. *Nat Chem Biol* 11(7):518–524.
7. Hui K, Liu B, Qin F (2003) Capsaicin activation of the pain receptor, VR1: Multiple open states from both partial and full binding. *Biophys J* 84(5):2957–2968.
8. Cui Y, et al. (2012) Selective disruption of high sensitivity heat activation but not capsaicin activation of TRPV1 channels by pore turret mutations. *J Gen Physiol* 139(4): 273–283.
9. Jordt SE, Julius D (2002) Molecular basis for species-specific sensitivity to "hot" chili peppers. *Cell* 108(3):421–430.
10. Gavva NR, et al. (2004) Molecular determinants of vanilloid sensitivity in TRPV1. *J Biol Chem* 279(19):20283–20295.
11. Liao M, Cao E, Julius D, Cheng Y (2013) Structure of the TRPV1 ion channel determined by electron cryo-microscopy. *Nature* 504(7478):107–112.
12. Cao E, Liao M, Cheng Y, Julius D (2013) TRPV1 structures in distinct conformations reveal activation mechanisms. *Nature* 504(7478):113–118.
13. Elokely K, et al. (2016) Understanding TRPV1 activation by ligands: Insights from the binding modes of capsaicin and resiniferatoxin. *Proc Natl Acad Sci USA* 113(2): E137–E145.
14. Darré L, Domene C (2015) Binding of capsaicin to the TRPV1 ion channel. *Mol Pharm* 12(12):4454–4465.
15. Hanson SM, Newstead S, Swartz KJ, Sansom MS (2015) Capsaicin interaction with TRPV1 channels in a lipid bilayer: Molecular dynamics simulation. *Biophys J* 108(6): 1425–1434.
16. Caterina MJ, Rosen TA, Tominaga M, Brake AJ, Julius D (1999) A capsaicin-receptor homologue with a high threshold for noxious heat. *Nature* 398(6726): 436–441.
17. Appendino G, Szallasi A (1997) Euphorbium: Modern research on its active principle, resiniferatoxin, revives an ancient medicine. *Life Sci* 60(10):681–696.
18. Zubcevic L, et al. (2016) Cryo-electron microscopy structure of the TRPV2 ion channel. *Nat Struct Mol Biol* 23(2):180–186.
19. Huynh KW, et al. (2016) Structure of the full-length TRPV2 channel by cryo-EM. *Nat Commun* 7:11130.
20. Hu HZ, et al. (2004) 2-Aminoethoxydiphenyl borate is a common activator of TRPV1, TRPV2, and TRPV3. *J Biol Chem* 279(34):35741–35748.
21. Ingólfsson HI, et al. (2014) Phytochemicals perturb membranes and promiscuously alter protein function. *ACS Chem Biol* 9(8):1788–1798.
22. Correll CC, Phelps PT, Anthes JC, Umland S, Greenfeder S (2004) Cloning and pharmacological characterization of mouse TRPV1. *Neurosci Lett* 370(1):55–60.
23. Lee BH, Zheng J (2015) Proton block of proton-activated TRPV1 current. *J Gen Physiol* 146(2):147–159.
24. Trudeau MC, Warmke JW, Ganetzky B, Robertson GA (1995) HERG, a human inward rectifier in the voltage-gated potassium channel family. *Science* 269(5220): 92–95.
25. Smith PL, Baukrowitz T, Yellen G (1996) The inward rectification mechanism of the HERG cardiac potassium channel. *Nature* 379(6568):833–836.
26. Sanguinetti MC, Tristani-Firouzi M (2006) hERG potassium channels and cardiac arrhythmia. *Nature* 440(7083):463–469.
27. Leaver-Fay A, et al. (2011) ROSETTA3: An object-oriented software suite for the simulation and design of macromolecules. *Methods Enzymol* 487:545–574.
28. Lemmon G, Meiler J (2012) Rosetta ligand docking with flexible XML protocols. *Methods Mol Biol* 819:143–155.
29. Yarov-Yarovoy V, Schonbrun J, Baker D (2006) Multipass membrane protein structure prediction using Rosetta. *Proteins* 62(4):1010–1025.
30. Zheng J, Ma L (2014) Structure and function of the thermoTRP channel pore. *Curr Top Membr* 74:233–257.
31. Appendino G, et al. (2003) Halogenation of a capsaicin analogue leads to novel vanilloid TRPV1 receptor antagonists. *Br J Pharmacol* 139(8):1417–1424.
32. Wahl P, Foged C, Tullin S, Thomsen C (2001) Iodo-resiniferatoxin, a new potent vanilloid receptor antagonist. *Mol Pharmacol* 59(1):9–15.
33. Catterall WA (2010) Ion channel voltage sensors: Structure, function, and pathophysiology. *Neuron* 67(6):915–928.
34. Sigworth FJ (1994) Voltage gating of ion channels. *Q Rev Biophys* 27(1):1–40.
35. Lu Z, Klem AM, Ramu Y (2002) Coupling between voltage sensors and activation gate in voltage-gated K^+ channels. *J Gen Physiol* 120(5):663–676.
36. Liu Y, Holmgren M, Jurman ME, Yellen G (1997) Gated access to the pore of a voltage-dependent K^+ channel. *Neuron* 19(1):175–184.
37. Yarov-Yarovoy V, et al. (2012) Structural basis for gating charge movement in the voltage sensor of a sodium channel. *Proc Natl Acad Sci USA* 109(2): E93–E102.
38. Long SB, Campbell EB, Mackinnon R (2005) Crystal structure of a mammalian voltage-dependent Shaker family K^+ channel. *Science* 309(5736):897–903.
39. Paulsen CE, Armache JP, Gao Y, Cheng Y, Julius D (2015) Structure of the TRPA1 ion channel suggests regulatory mechanisms. *Nature* 525(7570):552.
40. Salazar H, et al. (2009) Structural determinants of gating in the TRPV1 channel. *Nat Struct Mol Biol* 16(7):704–710.
41. Brederson JD, Kym PR, Szallasi A (2013) Targeting TRP channels for pain relief. *Eur J Pharmacol* 716(1-3):61–76.
42. Brown DC, et al. (2005) Physiologic and antinociceptive effects of intrathecal resiniferatoxin in a canine bone cancer model. *Anesthesiology* 103(5):1052–1059.
43. Karai L, et al. (2004) Deletion of vanilloid receptor 1-expressing primary afferent neurons for pain control. *J Clin Invest* 113(9):1344–1352.
44. Neubert JK, et al. (2005) Peripheral targeting of the trigeminal ganglion via the infraorbital foramen as a therapeutic strategy. *Brain Res Brain Res Protoc* 15(3): 119–126.
45. National Institutes of Health Clinical Center (National Institute of Dental and Craniofacial Research (2015) Resiniferatoxin to treat severe pain associated with advanced cancer. Available at https://clinicaltrials.gov/ct2/show/NCT00804154. Accessed March 10, 2016.
46. Caterina MJ, et al. (2000) Impaired nociception and pain sensation in mice lacking the capsaicin receptor. *Science* 288(5464):306–313.
47. Güler AD, et al. (2012) Transient activation of specific neurons in mice by selective expression of the capsaicin receptor. *Nat Commun* 3:746.
48. Sternson SM, Roth BL (2014) Chemogenetic tools to interrogate brain functions. *Annu Rev Neurosci* 37:387–407.
49. Cheng W, Yang F, Takanishi CL, Zheng J (2007) Thermosensitive TRPV channel subunits coassemble into heteromeric channels with intermediate conductance and gating properties. *J Gen Physiol* 129(3):191–207.
50. UniProt Consortium (2015) UniProt: A hub for protein information. *Nucleic Acids Res* 43(Database issue):D204–D212.
51. Hayes P, et al. (2000) Cloning and functional expression of a human orthologue of rat vanilloid receptor-1. *Pain* 88(2):205–215.
52. Savidge J, et al. (2002) Cloning and functional characterization of the guinea pig vanilloid receptor 1. *Neuropharmacology* 43(3):450–456.
53. Phelps PT, Anthes JC, Correll CC (2005) Cloning and functional characterization of dog transient receptor potential vanilloid receptor-1 (TRPV1). *Eur J Pharmacol* 513(1-2): 57–66.
54. Jahnel R, et al. (2003) Dual expression of mouse and rat VRL-1 in the dorsal root ganglion derived cell line F-11 and biochemical analysis of VRL-1 after heterologous expression. *Eur J Biochem* 270(21):4264–4271.
55. Sievers F, et al. (2011) Fast, scalable generation of high-quality protein multiple sequence alignments using Clustal Omega. *Mol Syst Biol* 7:539.
56. Waterhouse AM, Procter JB, Martin DM, Clamp M, Barton GJ (2009) Jalview Version 2—a multiple sequence alignment editor and analysis workbench. *Bioinformatics* 25(9):1189–1191.
57. Crooks GE, Hon G, Chandonia JM, Brenner SE (2004) WebLogo: A sequence logo generator. *Genome Res* 14(6):1188–1190.
58. Song Y, et al. (2013) High-resolution comparative modeling with RosettaCM. *Structure* 21(10):1735–1742.
59. Davis IW, Baker D (2009) RosettaLigand docking with full ligand and receptor flexibility. *J Mol Biol* 385(2):381–392.
60. Davis IW, Raha K, Head MS, Baker D (2009) Blind docking of pharmaceutically relevant compounds using RosettaLigand. *Protein Sci* 18(9):1998–2002.

61. Meiler J, Baker D (2006) ROSETTALIGAND: Protein-small molecule docking with full side-chain flexibility. *Proteins* 65(3):538–548.
62. Yarov-Yarovoy V, Baker D, Catterall WA (2006) Voltage sensor conformations in the open and closed states in ROSETTA structural models of K^+ channels. *Proc Natl Acad Sci USA* 103(19):7292–7297.
63. Kozlikova B, et al. (2014) CAVER Analyst 1.0: Graphic tool for interactive visualization and analysis of tunnels and channels in protein structures. *Bioinformatics* 30(18):2684–2685.
64. Pettersen EF, et al. (2004) UCSF Chimera—a visualization system for exploratory research and analysis. *J Comput Chem* 25(13):1605–1612.
65. Sakmann B, Neher E (2009) *Single-Channel Recording* (Springer, New York), 2nd Ed.
66. Sigworth FJ (1980) The variance of sodium current fluctuations at the node of Ranvier. *J Physiol* 307:97–129.
67. Yang F, Cui Y, Wang K, Zheng J (2010) Thermosensitive TRP channel pore turret is part of the temperature activation pathway. *Proc Natl Acad Sci USA* 107(15):7083–7088.